A Journal of the Gesellschaft Deutscher Chemiker

Angewandte Chemie

International Edition

GDCh

www.angewandte.org

2012–51/27

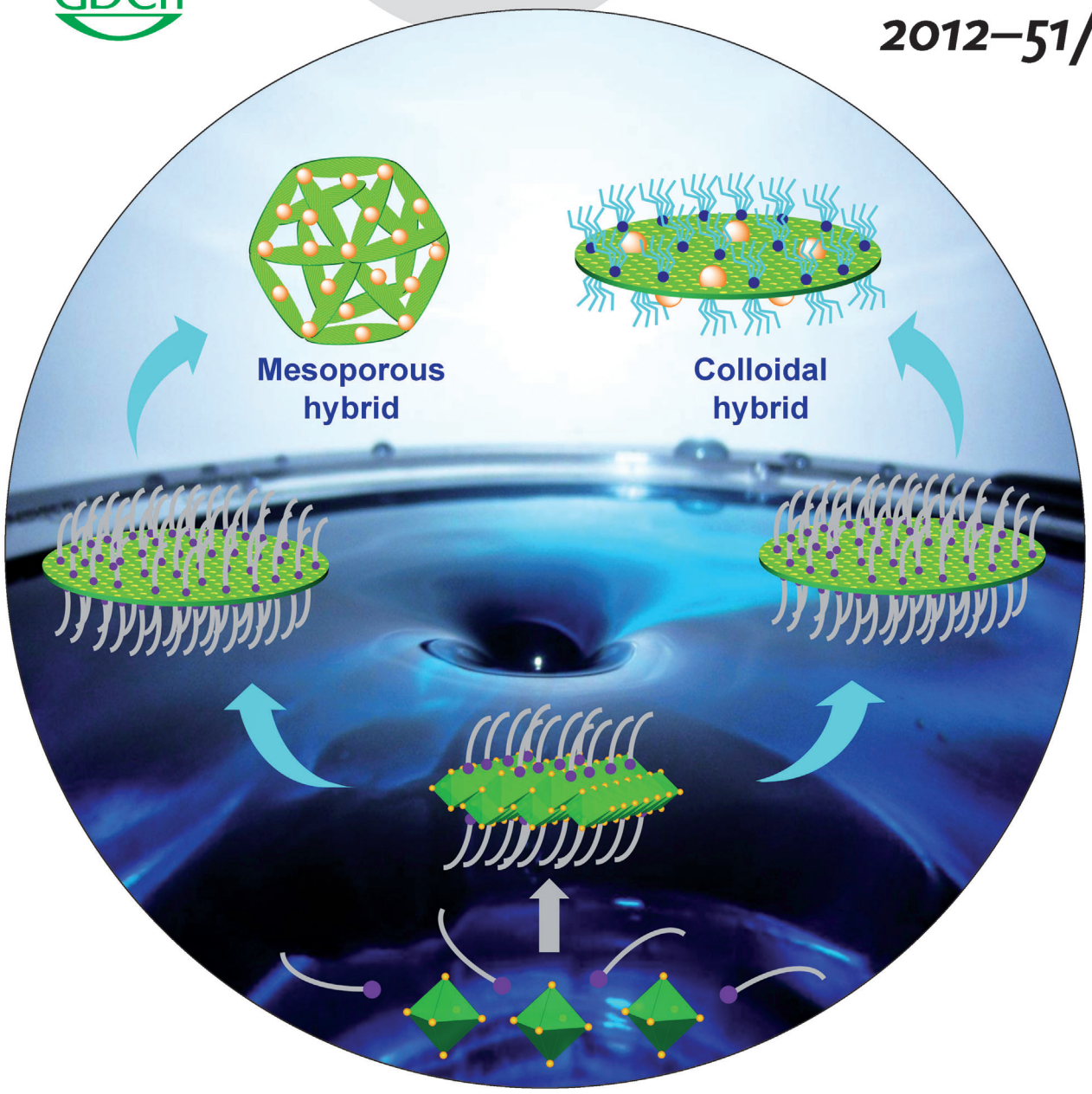

Inorganic nanocrystals ...

… play a central role in nanoscience and nanotechnology. In their Communication on page 6608 ff., F. Kleitz, T.-O. Do et al. present the bottom-up, non-aqueous synthesis of uniform titanate nanodisks with diameters of 12–35 nm. These nanodisks have been used as building blocks for a variety of hybrid nanostructures, such as titanate-based mesoporous hybrids with high surface areas and tailored porosity, as well as metal-titanate colloidal hybrids exhibiting enhanced catalytic activity.

WILEY-VCH

Hybrid Materials

DOI: 10.1002/anie.201202046

Controlled Synthesis of Titanate Nanodisks as Versatile Building Blocks for the Design of Hybrid Nanostructures**

Cao-Thang Dinh, Yongbeom Seo, Thanh-Dinh Nguyen, Freddy Kleitz, and Trong-On Do**

Inorganic nanocrystals with tailored particle morphology play a central role in nanoscience and nanotechnology owing to their unique physical and chemical features, which originate from size- and shape-dependent properties.[1] Furthermore, these nanocrystals can be used as building blocks for the construction of functional mesoscopic architectures that integrate desirable properties for a wide range of potential applications.[2]

Nanostructured titanate materials exhibiting various morphologies, for example, nanotubes, nanofibers, and nanosheets, among others, have attracted considerable attention owing to their excellent photo-electronic, catalytic, and mechanical properties.[3] These ion-exchangeable and highly photoactive nanostructures are considered to be promising for a wide range of applications, such as in Li batteries, catalytic oxidation reactions, ion adsorption, antibacterial coatings, and so on.[4] The prospects for the application of titanate materials are further extended by combining them with other nanoscopic domains, such as metal and semiconductor nanoparticles (NPs), to form multifunctional materials.[5] Among the different particle shapes, two-dimensional titanate nanosheets are attractive not only because of promising physical and chemical properties, for example, quantum confinement and surface effects, but also for the utility of these NPs in the assembly of new materials that possess long range mesoscopic periodicity. Following this approach, various nanostructures, including multilayer thin films, hollow nanocapsules, mesoporous hybrids, and so forth, have been constructed from titanate nanosheets.[5]

Conventionally, titanate nanosheets are prepared by chemical exfoliation of a parent layered titanate compound. This parent compound is synthesized either under hydrothermal conditions with a titanium precursor in concentrated alkali, or by calcining a mixture of a titanium precursor and alkali carbonate at high temperature.[6] However, the resulting titanate nanosheets are usually not uniform in shape and size; the lateral dimensions of the products range from a few hundred nanometers up to several micrometers.[6] Using these nanosheets as building blocks for hybrid assembly typically leads to mesoscopic structures of low order, and only very limited control of porosity is possible.

Herein, we report the synthesis of highly uniform colloidal titanate nanosheets exhibiting a plate-like shape, denoted as titanate nanodisks (TNDs), with exceptional size control (12–35 nm). These new TNDs are shown to be ideal building blocks for the fabrication of mesoporous titanate hybrids with a high surface area and easily tunable nanoporosity. These uniform TNDs can also be used as a stabilizer in the synthesis of ultra-small colloidal metal NPs, which exhibit enhanced catalytic properties, as compared to metal colloids stabilized by a conventional organic protecting agent.

In our approach, TNDs resulted from the reaction of titanium butoxide (TB), benzyl alcohol (BA), and oleylamine (OM) under nonhydrolytic conditions. Uniform titanate nanodisks were synthesized by heating a mixture of TB, OM, and BA in benzyl ether at 190 °C for 20 h. The diameter of the resulting nanodisks can be tuned by simply changing the amount of BA used, while keeping other conditions unchanged. For example, to synthesize TNDs with a ca. 22 nm diameter, TB (2 g), OM (12 g), BA (12 g), and benzyl ether (30 g) were used (see the Supporting Information). Figure 1 shows transmission electron microscopy (TEM) images of the resulting TNDs, which are highly uniform in size and have a mean diameter of 22 nm (Figure 1 a,b). Because of the ultrathin structure of TNDs, these NPs tend to lay parallel to the grid surface. To estimate the thickness of the TNDs, a precipitate of TNDs in ethanol was used for TEM analysis (Figure 1 d,e). Under these conditions, the nanodisks self-assembled in ethanol, producing a lamellar structure made up of TNDs. The images show that the TNDs are ultrathin, with a thickness of 0.75 nm (Figure 1 e).

High resolution (HR) TEM was used to verify the crystalline structure of the TNDs. As shown in Figure 2 a,b, the HRTEM images of TNDs laying parallel to the TEM grid revealed a crystalline lattice with 0.19 and 0.15 nm interplanar spacings along the *a* and *b* axes, respectively. HRTEM images of TNDs assembled in ethanol and oriented parallel to the

[*] C.-T. Dinh, T.-D. Nguyen, Prof. T.-O. Do
Department of Chemical Engineering and Centre de recherche sur les propriétés des interfaces et la catalyse
Laval University, Quebec, G1V0A6 (Canada)
E-mail: trong-on.do@gch.ulaval.ca
Prof. F. Kleitz
Department of Chemistry and Centre de Recherche sur les Matériaux Avancés
Laval University, Quebec, G1V0A6 (Canada)
E-mail: freddy.kleitz@chm.ulaval.ca
Y. Seo
Department of Chemistry and Graduate School of Nanoscience and Technology, KAIST (Republic of Korea)

[**] This work was supported by the Natural Sciences and Engineering Research Council of Canada (NSERC). Y.S. acknowledges support from the National Research Foundation (National Honor Scientist Program 20110031411 and the World Class University Program R312011000100710) in Korea. C.T.D. thanks les fonds de recherche du Québec (FQRNT) for an Excellence Scholarship. The authors wish to thank Prof. Ryong Ryoo (KAIST, Korea) for access to a high resolution TEM microscope.

Supporting information for this article is available on the WWW under http://dx.doi.org/10.1002/anie.201202046.

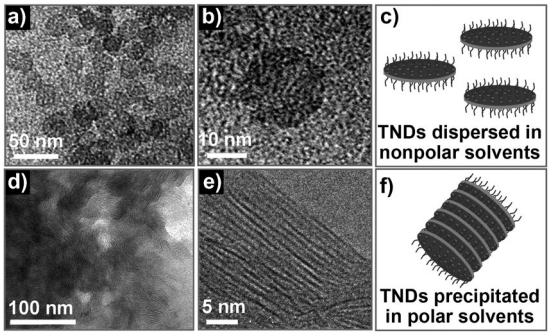

Figure 1. Solvent effects on titanium nanodisks. a–c) TNDs in nonpolar solvents; a,b) TEM images of TNDs dispersed in toluene, c) illustration of TND organization in toluene. d–f) TNDs in polar solvents; d,e) TEM images of TNDs precipitated in ethanol, f) illustration of TND organization in ethanol.

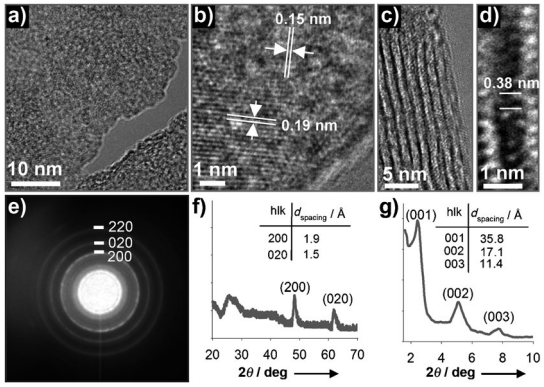

Figure 2. Analysis of precipitated TNDs. a,b) HRTEM images of TNDs laying perpendicular to the electron beam. c,d) HRTEM images of TNDs laying parallel to the beam. e) SAED of a single TND. f,g) XRD patterns of TNDs; f) wide-angle, g) low-angle.

direction of the electron beam (Figure 2c,d) showed a periodic atomic arrangement along the *a* axis with a spacing of 0.38 nm, which is twice the spacing along the *a* axis (0.19 nm). Furthermore, uniform stacking of TNDs along the *c* axis is visible (Figure 2c), and the spacing between the TNDs was ca. 2.2 nm, which is a little larger than the length of the oleylamine surfactant layers. The HRTEM analyses revealed that the TNDs are lepidocrocite-type titanate with lateral unit cell dimensions of 0.38 and 0.3 nm, which correspond to the *a* and *b* axes of the unit cell, respectively (Supporting Information, Figure S1).[7]

The crystal structure of the TNDs was further characterized by selected area electron diffraction (SAED) and powder X-ray diffraction (XRD). As depicted in Figure 2e, the SAED pattern of a single TND laying parallel to the grid surface clearly showed three rings, which can be indexed as (200), (020), and (220). The center-to-200/center-to-020 distance ratio was 15:19, which coincides well with the inverse ratio of the interplanar spacing along the *a* (0.19 nm) and *b* (0.15 nm) axes. The wide angle XRD pattern of TNDs assembled in a nonpolar solvent showed the presence of two peaks located at 48.3° and 62.0°, corresponding to interplanar distances of 0.19 and 0.15 nm, respectively, in the TNDs. The low-angle XRD pattern of the TND powder exhibited diffraction peaks at 2.5°, 5.1°, and 7.9°, which can be indexed to the (001), (002), and (003) planes, respectively. These diffraction peaks are characteristic of a lamellar mesoscopic structure. The XRD basal distance of 3.23 nm, corresponding to the (001) peak, is in good agreement with the HRTEM results.

To ascertain the chemical formula of the TNDs, the amount of OM in the TNDs synthesized by the aforementioned procedure was estimated by TGA. The result revealed that about 40 wt% of OM is present in the as-synthesized TNDs (Figure S2). From this result, it can be approximated that the OM/Ti molar ratio in TNDs was close to 1:3. However, considering the fact that OM can be physically adsorbed on the surface of TNDs, the number of OM molecules contributing to the chemical formula of the TNDs may be slightly different. High resolution X-ray photoelectron spectroscopy (XPS) can be used to determine the OM/Ti ratio more accurately, as well as identifying the protonated state of the OM amine groups.[8] As shown in Figure S3 of the Supporting Information, the high resolution N1s XPS spectrum of TNDs exhibits two peaks at binding energies of 401.5 eV and 399.6 eV. The major peak at the higher binding energy can be attributed to protonated nitrogen, while the minor one at the lower binding energy originates from free OM molecules adsorbed on the surface of the TNDs.[8] From this data, the molar ratio of protonated OM to free OM is 2.1:1. The chemical formula of a lepidocrocite-type titanate is often represented as $M_xTi_{2-x/4}\diamond_{x/4}O_4$ (M = monovalent cation, $\diamond$ = titanium vacancy).[6c,7] Thus, based on the XPS and TG results, it can be concluded that the OM/Ti molar ratio in the TNDs was 1:4.7. Therefore, the unit cell formula of the as-synthesized TNDs can be described as $(OM)_{0.4}Ti_{1.9}\diamond_{0.1}O_4$.

The OM and BA species play crucial roles in the formation of TNDs. The reaction between TB and BA yields TiO_6 octahedra, which form the primary building units of TNDs, while OM, protonated at elevated temperature by BA, balances the negative charge of the TNDs. In the absence of BA no NPs were formed, while in the absence of OM a large amount of anatase TiO_2 NPs were produced, as shown in the Supporting Information Figures S4 (TEM, ESI) and S5 (XRD, ESI). These results confirmed that the presence or absence of OM controls the formation of either the titanate phase or anatase, respectively. This effect may be related to the protonation of OM molecules by BA at high temperature, resulting in protonic OM, which induces formation of the titanate. Furthermore, it has been reported that BA can be used as a medium for the formation of a variety of metal oxides.[9] In previous cases, nonhydrolytic reaction between TB and BA led to TiO_6 octahedra that served as building units for titanium oxide materials.[9a] Therefore, the amount of BA used may directly affect the crystallization process of TNDs, and consequently, the size of the resulting TNDs. To further confirm this, we have also performed the synthesis of TNDs using different amounts of BA while keeping other conditions unchanged. It was found that TNDs with a size of around 12 nm were obtained when a smaller amount of BA (6 g) was used (Figure S6). When a larger amount of BA (24 g) was

used, TNDs with a diameter of about 35 nm were produced (Figure S7). A further increase in the amount of BA (36 g) resulted in the formation of a mixture of large TNDs and anatase TiO_2 NCs (Figure S8). This result may be due to the faster formation of TiO_6 octahedra, which is favorable for the generation of the anatase phase. These findings establish that the size of TNDs can finely be tuned by simply changing the amount of BA used in the the synthesis. This fact is significant because TNDs with different diameters will be of special interest when used as building blocks for the formation of nanostructured hybrids, as this can result in hybrid materials with a variety of structures.

The as-synthesized TNDs (OM-TNDs) are highly dispersed in a non-polar solvent (for example, toluene), which is a property rarely found for layered titanate materials (Figure S9a). Moreover, these TNDs can also be cation-exchanged with tetraethylammonium (TEA) salts, leading to TEA-exchanged TNDs (TEA-TNDs) that are readily dispersed in water (Figure S9b). FTIR analyses performed on TNDs after treatment with TEA showed no absorption band at 3004 cm^{-1}, which would correspond to the stretching vibration of the C–H bond in the C=C group of the OM molecules[10] (Figure S10). This result indicates that the OM molecules adsorbed on the surface of the TNDs have been fully displaced by the TEA cations. The TEA-TNDs so obtained were used as precursors for the design of various titanate-based hybrid nanostructures. TEA-TNDs dispersed in water showed a very high ion-exchange rate. Depending on the amount of metal cations used to exchange with TEA, two different types of titanate-based hybrids could be created, mesoporous or colloidal. For the synthesis of mesoporous hybrids, an excess of the metal (metal/titanium atomic ratio of 1:2) was used. Accordingly, TEA-TNDs dispersed in water were added to a solution of metal cations, such as Ag^+, Cu^{2+} or Cd^{2+}, leading to rapid precipitation of metal-ion-exchanged TNDs (for example, Ag^+ TNDs, Cu^{2+} TNDs, Cd^{2+} TNDs; Supporting Information, Figure S9c). As a representative example, the ion exchange process to generate Ag^+TNDs was completed within 20 min and the sample FTIR spectrum showed no hydrocarbon group peaks, indicating that the TEA cations have been completely displaced by the metal ions (Supporting Information, Figure S10).

These metal-ion-exchanged TNDs could then be converted into the corresponding mesoporous titanate hybrids. For example, a mesoporous Ag_2O–titanate hybrid was formed by aging the Ag^+TNDs precipitate in a sodium hydroxide solution at room temperature overnight. The brown precipitate was then dried at 150 °C for 10 h. Figure 3a,b shows TEM images of the Ag_2O–titanate hybrid synthesized from TNDs of 22 nm diameter (Ag_2O-titanate-22). This Ag_2O-titanate-22 hybrid is clearly a highly porous material (Figure 3a). A high magnification TEM image taken on the edge of a Ag_2O-titanate-22 particle (Figure 3b) revealed that this material consists of TNDs and Ag_2O NPs. It is believed that the Ag_2O NPs grew on each TND due to the adsorption of Ag^+ on all of the TNDs as a result of the high dispersion of TNDs in water. The Ag_2O–TND hybrid particles are assembled in the form of a mesoporous Ag_2O–titanate hybrid, in which titanate and Ag_2O domains are uniformly distributed

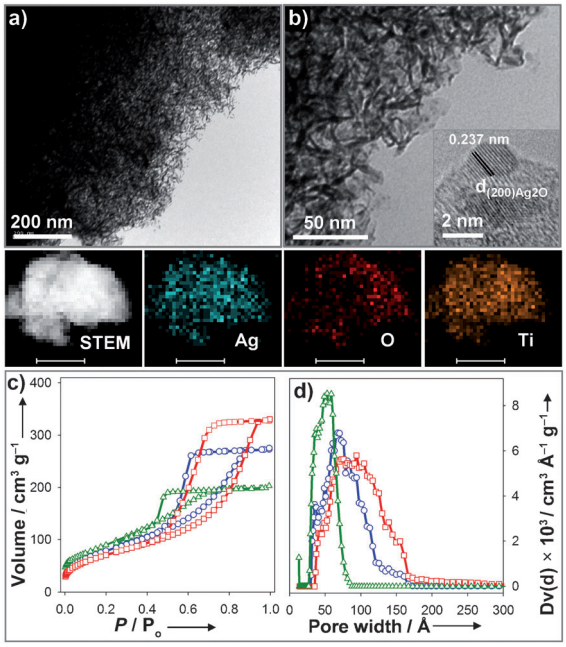

Figure 3. Analysis of Ag_2O–titanate hybrids. a,b) TEM images of Ag_2O–titanate hybrids synthesized from TNDs of 22 nm diameter (Ag_2O-titanate-22) showing the presence of Ag_2O NPs; a) low magnification, b) high magnification and HRTEM (inset). Middle panel shows elemental mapping of Ag_2O–titanate hybrids; scale bars are 1 μm. c) N_2 physisorption isotherms of Ag_2O–titanate hybrids synthesized from TNDs with different particle diameters. d) Corresponding NLDFT pore size distributions (adsorption branch). Ag_2O-titanate-35 (—□—), Ag_2O-titanate-22 (—○—), Ag_2O-titanate-12 (—△—).

throughout the hybrid network, as indicated by elemental mapping (Figure 3, middle panel). Further, the chemical state of silver in the Ag_2O-titanate-22 hybrid was verified by XPS (Figure S11a). The peak located at a binding energy of 367.6 eV, observed on the XPS Ag 3d spectrum of Ag_2O-titanate-22, is characteristic of Ag_2O crystals.[11] According to elemental analysis performed by energy-dispersive X-ray spectroscopy (Figure S11b), the atomic ratio of Ag/Ti here is 1:4.5, which is in line with the molar ratio of OM/Ti (1:4.7) in the as-synthesized TNDs.

The N_2 adsorption-desorption isotherms of the Ag_2O-titanate-22 hybrids, depicted in Figure 4c, show a type IV isotherm behavior with a H2 hysteresis loop, which is characteristic of mesoporous materials with large cage-like or ink-bottle-type pores.[12] The BET specific surface area of these hybrids reaches 290 $m^2 g^{-1}$. Interestingly, the porosity of the resulting hybrids could be reproducibly tuned by using TNDs with different sizes as building blocks. When TNDs with a diameter of 12 nm were used, the resulting hybrid (Ag_2O-titanate-12) exhibited a higher surface area (320 $m^2 g^{-1}$), but a lower pore volume (Figure 3c). In contrast, using TNDs with a diameter of 35 nm as building blocks resulted in a mesoporous Ag_2O-titanate-35 hybrid with a higher pore volume (Figure 3c), but with a lower surface area (270 $m^2 g^{-1}$). The pore size distribution analysis, calculated by the NLDFT method (adsorption branch), shown in Figure 3d, revealed that, as the diameter of the TND building

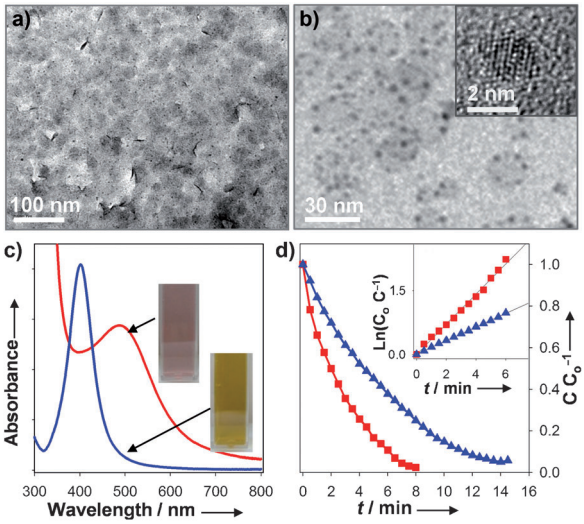

Figure 4. Comparison of TND-stabilized and PVP-stabilized Ag NPs. a,b) TEM images of TND-stabilized Ag NPs; a) low magnification, b) high magnification and HRTEM image (inset). (c) UV–Vis absorption spectra of TND-stabilized and PVP-stabilized NPs; TND-stabilized Ag NPs (——), PVP-stabilized Ag NPs (——); inset shows photos of the corresponding NPs dispersed in water. (d) Variation of MB concentration vs. reaction time for TND-stabilized and PVP-stabilized NPs; inset shows plots of $\ln(C_o/C)$ vs. reaction time showing the fit using a first order reaction rate; TND-stabilized Ag NPs (■), PVP-stabilized Ag NPs (▲).

blocks increased from 12 nm to 22 nm and then to 35 nm, the average pore size of the resulting hybrids increased noticeably from 4.9 nm to 6.8 nm and then to 9.3 nm, respectively. Further, we have also used the TNDs as building blocks to prepare Ag–titanate, Cu_xO–titanate, and CdS–titanate mesoporous hybrids (Figure S12–14) with BET surface areas between 250 and 280 m^2g^{-1} (Table S1). These results are among the highest values thus far reported for mesoporous hybrids derived from titanate nanosheets, which could be of great interest for catalytic and photocatalytic applications.

Similarly, colloidal metal NPs stabilized by TNDs were obtained by controlling the amount of metal ions added to a dispersion of TEA-TNDs, followed by reduction of the metal cations adsorbed on the TND surface. For Ag NPs, a solution containing Ag^+ ions was added to TEA-TNDs dispersed in water (Ag/Ti atomic ratios of 1:30). The TND dispersion remained colorless after addition of Ag^+, but changed from colorless to light brown and finally to pink upon addition of the reducing agent (tetraethylborohydride), which is indicative of the formation of metal NPs. No additional capping agent was used to stabilize the Ag NPs. The resulting Ag NPs stabilized by TNDs remained stable over several months without any noticeable precipitation. A control experiment without TNDs, but otherwise carried out under the same conditions, resulted in a brown precipitate of Ag particles 30 min after the addition of the reducing agent.

Figure 4a,b shows representative TEM and HRTEM images of Ag NPs stabilized by TNDs. It can be seen that the resulting Ag NPs exhibit a uniform size in the range of 2–3 nm. For comparison, colloidal Ag NPs stabilized by polyvinylpyrrolidone (PVP) instead of TNDs were also prepared under otherwise identical conditions. TEM investigations indicated the formation of less uniform PVP-stabilized Ag NPs with sizes in the range of 5–20 nm (Figure S15). To explain the formation of metal NPs stabilized by TNDs, we can speculate that introducing Ag^+ to the solution of TEA-TNDs leads to only a partial replacement of TEA^+ by Ag^+ on the TND surface. Upon the addition of a reducing agent, Ag^+ ions are reduced in situ on the surface of the TNDs to form very small Ag NPs. Figure 4c shows the UV–Vis absorption spectra of both PVP-stabilized and TND-stabilized Ag NPs. The UV–Vis spectrum of the TND-stabilized Ag NPs shows a peak maximum at 482 nm, which is 82 nm red-shifted versus that of the PVP-stabilized Ag NPs (400 nm). This may be attributed to the high dielectric constant of TNDs, as the peak maximum of colloidal metal NPs is known to be red-shifted as the value of the dielectric constant of their surrounding matrix increases.[13]

The PVP-stabilized and TND-stabilized Ag NPs were further used to catalyze the reduction of methylene blue (MB) by a borohydride compound in the aqueous phase.[14] The results indicated that the TND-stabilized Ag NPs clearly exhibit a much higher catalytic activity than their PVP-stabilized counterparts (Figure 4d). MB was fully reduced by TND-stabilized Ag NPs within 7 min of reaction. In contrast, the reaction with PVP-stabilized Ag NPs took twice the time, 14 min, to completely reduce MB in solution. The rate constant (k) for the reduction of MB over TND-stabilized Ag NPs, calculated with a first order reaction kinetics model $[\ln(C_o/C) = kt]$, was 0.347 min^{-1}, which is double the value calculated for PVP-stabilized Ag NPs (0.161 min^{-1}). Furthermore, it is known that colloidal metal NPs tend to suffer from activity loss during reaction, an effect which is caused by aggregation.[15] In contrast, TND-stabilized Ag NPs maintained high activity over five consecutive reduction cycles (Figure S16). TEM and XRD analyses of the TND-stabilized Ag NPs showed no detectable morphological and crystallite phase change after five cycles (Figure S17). Thus, the presence of TNDs seems to provide efficient stabilization of the Ag NP catalyst by preventing particle aggregation.

The use of TNDs as effective stabilizers was extended to the synthesis of other metal NPs. As shown in Figure S18 and 19, TND-stabilized Cu and Ni NPs with a uniform size of about 2 nm could also be obtained. Furthermore, the TNDs can act as stabilizers for non-metal inorganic NP compositions as well. For example, AgBr NPs could be synthesized and exhibited a particle size of 4 nm (Figure S20).

In summary, we have developed a new, non-aqueous route for the synthesis of ultrathin TNDs with a controlled particle diameter in the range of 12–35 nm. These TNDs are uniform in size and shape and can be used as building blocks for the design of a variety of mesoporous hybrids with a high surface area and controlled porosity, which is of great importance for catalytic applications. We have also demonstrated the use of uniform titanate nanosheets as stabilizers for the synthesis of ultra-small colloidal metal NPs without the use of other protecting agents. These metal NPs are stabilized by TNDs to form colloidal metal–TND hybrids, and exhibited remarkable catalytic properties in terms of both activity and stability. It is thus expected that these TNDs could be promising building

units for the design of various sophisticated nanostructures, which could have great potential for electronic, photochemical, and catalytic applications.

Received: March 14, 2012
Published online: May 25, 2012

Keywords: building blocks · mesoporous materials · nanoparticles · nanostructures · titanates

[1] a) Y. Sun, Y. Xia, *Science* **2002**, *298*, 2176; b) Y. Xia, Y. Xiong, B. Lim, S. E. Skrabalak, *Angew. Chem.* **2008**, *121*, 62; *Angew. Chem. Int. Ed.* **2008**, *48*, 60; c) Y. W. Jun, J. S. Choi, J. Cheon, *Angew. Chem.* **2006**, *118*, 3492; *Angew. Chem. Int. Ed.* **2006**, *45*, 3414; d) C. T. Dinh, T. D. Nguyen, F. Kleitz, T. O. Do, *ACS Nano* **2009**, *3*, 3737.

[2] a) D. V. Talapin, J. S. Lee, M. V. Kovalenko, E. V. Shevchenko, *Chem. Rev.* **2010**, *110*, 389; b) M. Rycenga, C. M. Cobley, J. Zeng, W. Li, C. H. Moran, Q. Zhang, D. Qin, Y. Xia, *Chem. Rev.* **2011**, *111*, 3669.

[3] a) T. Sasaki, M. Watanabe, H. Hashizume, H. Yamada, H. Nakazawa, *J. Am. Chem. Soc.* **1996**, *118*, 8329; b) M. Osada, Y. Ebina, H. Funakubo, S. Yokoyama, T. Kiguchi, K. Takada, T. Sasaki, *Adv. Mater.* **2006**, *18*, 1023; c) M. Kitano, K. Nakajima, J. N. Kondo, S. Hayashi, M. Hara, *J. Am. Chem. Soc.* **2010**, *132*, 6622; d) A. Antonello, M. Guglielmi, V. Bello, G. Mattei, A. Chiasera, M. Ferrari, A. Martucci, *J. Phys. Chem. C* **2010**, *114*, 18423; e) A. Antonello, G. Brusatin, M. Guglielmi, V. Bello, G. Petrotto, G. Mattei, M. Maiwald, V. Zöllmer, A. Chiasera, M. Ferrari, A. Marticci, *Opt. Mater.* **2011**, *33*, 1839.

[4] a) A. R. Armstrong, G. Armstrong, J. Canales, P. G. Bruce, *Angew. Chem.* **2004**, *116*, 2336; *Angew. Chem. Int. Ed.* **2004**, *43*, 2286; b) A. Riss, M. J. Elser, J. Bernardi, O. Diwald, *J. Am. Chem. Soc.* **2009**, *131*, 6198; c) S. N. Britvin, A. Lotnyk, L. Kienle, S. V. Krivovichev, W. Depmeier, *J. Am. Chem. Soc.* **2011**, *133*, 9516; d) Y. Ide, M. Ogawa, *Angew. Chem.* **2007**, *119*, 8601; *Angew. Chem. Int. Ed.* **2007**, *46*, 8449; e) D. Yang, S. Sarina, H. Zhu, H. Liu, Z. Zheng, M. Xie, S. V. Smith, S. Komarneni, *Angew. Chem.* **2011**, *123*, 10782; *Angew. Chem. Int. Ed.* **2011**, *50*, 10594; f) D. Portehault, C. Giordanot, C. Sanchez, M. Antonietti, *Chem. Mater.* **2010**, *22*, 2125.

[5] a) R. Ma, T. Sasaki, *Adv. Mater.* **2010**, *22*, 5082; b) T. W. Kim, S. J. Hwang, S. H. Jhung, J. S. Chang, H. Park, W. Choi, J. H. Choy, *Adv. Mater.* **2008**, *20*, 539; c) M. Osada, T. Sasaki, *Adv. Mater.* **2012**, *24*, 210.

[6] a) C. Y. Xu, Q. Zhang, H. Zhang, L. Zhen, J. Tang, L. C. Qin, *J. Am. Chem. Soc.* **2005**, *127*, 11584; b) T. Tanaka, Y. Ebina, K. Takada, K. Kurashima, T. Sasaki, *Chem. Mater.* **2003**, *15*, 3564; c) T. Sasaki, Y. Ebina, Y. Kitami, M. Watanabe, T. Oikawa, *J. Phys. Chem. B* **2001**, *105*, 6116.

[7] a) N. Sakai, Y. Ebina, K. Takada, T. Sasaki, *J. Am. Chem. Soc.* **2004**, *126*, 5851; b) E. L. Tae, K. E. Lee, J. S. Jeong, K. B. Yoon, *J. Am. Chem. Soc.* **2008**, *130*, 6534.

[8] a) C. T. Dinh, T. D. Nguyen, F. Kleitz, T. O. Do, *Chem. Commun.* **2011**, *47*, 7797; b) F. Zhang, M. P. Srinivasan, *Langmuir* **2004**, *20*, 2309.

[9] a) D. Koziej, F. Fischer, N. Kranzlin, W. R. Caseri, M. Niederberger, *ACS Appl. Mater. Interfaces* **2009**, *1*, 1097; b) M. Niederberger, M. H. Bartl, G. D. Stucky, *J. Am. Chem. Soc.* **2002**, *124*, 13642; c) N. Pinna, M. Niederberger, *Angew. Chem.* **2008**, *120*, 5372; *Angew. Chem. Int. Ed.* **2008**, *47*, 5292.

[10] E. Kinder, P. Moroz, G. Diederich, A. Johnson, M. Kirsanova, A. Nemchinow, T. O'Connor, D. Roth, M. Zamkov, *J. Am. Chem. Soc.* **2011**, *133*, 20488.

[11] X. Wang, S. Li, H. Yu, J. Yu, S. Liu, *Chem. Eur. J.* **2011**, *17*, 7777.

[12] F. Kleitz, T. Czuryszkiewicz, L. A. Solovyov, M. Lindén, *Chem. Mater.* **2006**, *18*, 5070.

[13] a) N. Sandhyarani, M. R. Resmi, R. Unnikrishnan, K. Vidyasagar, S. Ma, M. P. Antony, G. P. Selvam, V. Visalakshi, N. Chandrakumar, K. Pandian, Y. T. Tao, T. Pradeep, *Chem. Mater.* **2000**, *12*, 104; b) L. M. L. Marzán, M. Giersig, P. Mulvaney, *Langmuir* **1996**, *12*, 4329.

[14] a) N. R. Jana, T. Pal, *Langmuir* **1999**, *15*, 3458; b) A. C. Patel, S. X. Li, C. Wang, W. J. Zhang, Y. Wie, *Chem. Mater.* **2007**, *19*, 1231.

[15] R. Narayanan, M. A. El-Sayed, *J. Am. Chem. Soc.* **2003**, *125*, 8340.

Angewandte Chemie
Eine Zeitschrift der Gesellschaft Deutscher Chemiker

Supporting Information

69451 Weinheim, Germany

Controlled Synthesis of Titanate Nanodisks as Versatile Building Blocks for the Design of Hybrid Nanostructures**

Cao-Thang Dinh, Yongbeom Seo, Thanh-Dinh Nguyen, Freddy Kleitz, and Trong-On Do**

anie_201202046_sm_miscellaneous_information.pdf

Supporting Information

Experimental section

Chemicals: All chemicals were used as received; Titanium butoxide (TB), benzyl alcohol (BA), oleylamine (OM), benzyl ether, tetraethylammonium (TEA) hydroxide, silver nitrate, copper nitrate, cadmium nitrate, sodium hydroxide, disodium sulfide, methylene blue (MB), and tetraethylammonium borohydride were purchased form Aldrich. Absolute ethanol and toluene solvents were of analytical grade and were also purchased form Aldrich.

Synthesis of titanate nanodisks (TNDs) with diameter of ca. 22 nm: To synthesize TNDs with diameter of ~ 22 nm, 2g of TB, 12 g of OM, 12g of BA (OM:BA weight ratio of 1:1), and 30g of benzyl ether were added to a 100-mL round-bottom flask. The reaction mixture was heated to 190 ^{o}C at the heating rate 5 ^{o}C/min under nitrogen flow. After 20 h, the reaction was stopped and cooled down to room temperature. After addition of excess absolute ethanol, the TNDs were obtained by centrifugation and redispersed in toluene for microscope analysis.The obtained nanodisks were then re-dispersed in toluene and re-precipitated by ethanol. This process was repeated three times to remove the un-reacted reagents.

Synthesis of titanate nanodisks with different diameters: The procedures for the synthesis of 12 nm-, and 35 nm-diameter TNDs were similar to that of 22 nm-diameter TNDs, except that 6g and 24g of BA were used, respectively.

Tetraethylammonium and metal cations exchanged titanate nanodisks: The as-synthesized TNDs were treated with tetraethyl ammonium hydroxide to obtain TEA-TNDs. Typically, 5 mmol of as-synthesized TNDs (according to Ti atom) were dispersed in a mixture of TEAOH (15 mmol), ethanol (15 ml) and water (15 ml). The mixture was stirred overnight at room temperature. To the clear solution obtained was added access

acetone to precipitate TNDs. The precipitate was then washed several times with acetone and finally dispersed in 10 ml of water.

Synthesis of titanate based mesoporous hybrids: To synthesize titanate based mesoporous hybrids, first, metal cations exchanged TNDs were prepared. Accordingly, the TEA-TNDs dispersed in water was gradually added to a solution contain metal cations (Ag^{+}, Cd^{2+}, Cu^{2+}) (metal : titanium atomic ratio of 1:2) under stirring condition. The resulting precipitates (metal exchanged TNDs: Ag^{+}-TNDs, Cd^{2+}-TNDs, Cu^{2+}-TNDs) were then washed several times with water to remove un-exchanged cations. To synthesize mesoporous Ag_2O-titanate and CuO_x-titanate hybrids, Ag^{+}-TNDs, and Cu^{2+}-TNDs were immersed in a NaOH solution (0.1N) overnight. The obtained powders was then washed several times with water and dried at 150 ^{o}C for 5 h. The procedure for the synthesis of mesoporous CdS-titanate hybrid was similar to that of Ag_2O-titanate, except that Na_2S solution was used instead of NaOH. Mesoporous Ag-titanate hybrid was obtained by reducing Ag^{+} in Ag^{+}-TNDs using $NaBH_4$.

Synthesis of TND-stabilized metal NPs: to 50 ml solution containing 5 mmol TNDs was added 10 ml of metal nitrate solution (Ag, Cu, Ni, metal : titanium atomic ratio of 1:30) under stirring condition. The mixture was stirred for 60 min and then was added with the reducing agent (tetraethylammonium borohydride, TEABH). (TEABH : metal molar ratio of 5:1). A clear solution of the metal NPs stabilized by TNDs were obtained after another 60 min of stirring. For the synthesis of AgBr NPs stabilized by TNDs (AgBr-TNDs hybrid colloids), tetraethylammonium bromide was used instead of TEABH).

Synthesis of PVP-stabilized Ag NPs: The procedure for the synthesis of PVP-stabilized Ag NPs was similar to that of TND-stabilized Ag NPs, except that 50 ml solution containing PVP (0.3 g) was used instead of TNDs. The molar concentration of silver in PVP-stabilized Ag NPs solution was equal to that in TND-stabilized Ag NPs solution.

Characterization: Transmission electron microscopy (TEM) images of TNDs were obtained on a JOEL JEM 1230 operated at 120kV. High resolution TEM images were performed on Philips G2 F30 Tecnai instrument operated at 300kV. XPS measurements were carried out in an ion-pumped chamber (evacuated to 10-9 Torr) of a photoelectron spectrometer (Kratos Axis-Ultra) equipped with a focused X-ray source (Al Kα, hv = 1486.6 eV). Powder X-ray diffraction patterns of the samples were obtained on a Bruker SMART APEXII X-ray diffractometer equipped with a Cu Kα radiation rource (λ=1.5418 Å). The thermal analyses of the as-made TNDs were carried out at a heating rate of 10 °C/min under a oxygen flow up to 700 °C using a Perkin-Elmer TGA thermogravimetric analyzer. The UV-vis spectra were recorded on a Cary 300 Bio UV-visible spectrophotometer. Fourier transform infrared (FTIR) absorption spectra were measured with a FTS 45 infrared spectrophotometer with the KBr pellet technique. N_2 adsorption-desorption isotherms of the samples were measured at -196 ^{o}C using Micromeretics ASAP 2010 instrument. Before the measurements, the samples were outgassed under vacuum for 6 h at 150 °C. The total pore volume (V_{pore}) was calculated from the amount of nitrogen adsorbed at P/P_0 = 0.95. The model used for the NLDFT evaluations was N_2 adsorbed on silica (spherical pore geometry) considering the adsorption branch.[12]

Catalytic study: A model aqueous phased reduction of methylene blue (MB) using tetraethylammonium borohydride (TEABH) was used to test the catalytic activity of Ag NPs stabilized by TNDs and PVP. First, aqueous solutions of MB (10 mM) and TEABH (2M) were prepared. 1 ml of TND (or PVP)-stabilized Ag NP solution and 1 ml of distilled water was added into a 4ml quartz cuvette. To this mixture was added 30µl of TEABH solution, the obtained solution was then purged with nitrogen gas for 10 min. After that, 30µl of MB solution was added to the cuvette to start the reaction and the absorption peak at 664nm was monitored by UV-vis spectroscopy as a function of time. After the first run, another 30µl of TEABH solution was added into the cuvette. The mixture was then purged with nitrogen gas for 10 min. After that, 30µl of MB solution was added to start the second cycle of reaction. This step was repeated 4 times to study the stability of the catalysts.

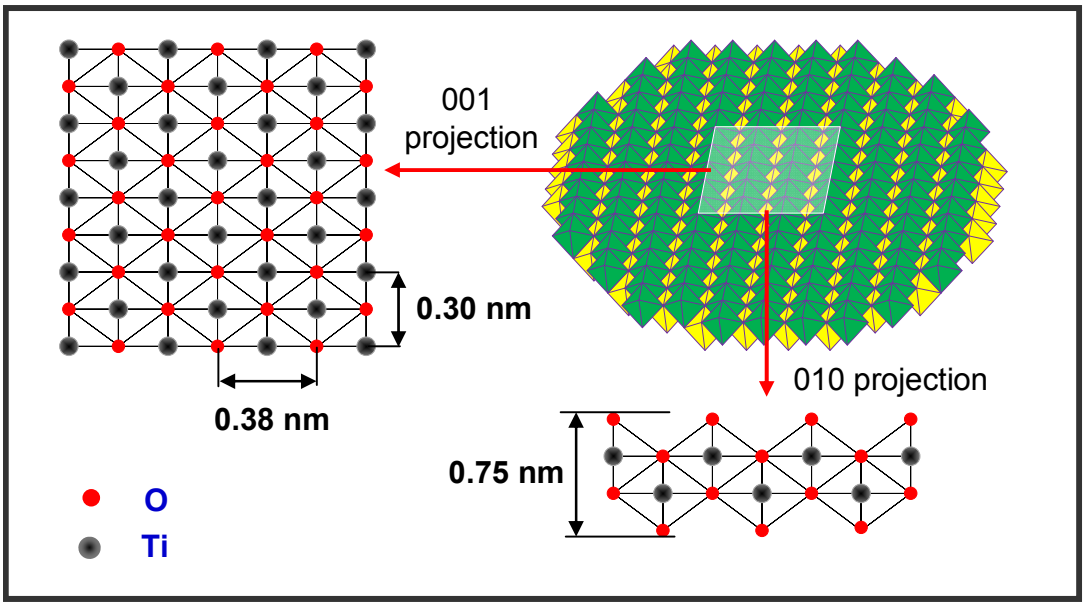

Figure S1. Schematic illustration in perspective view of TND and projections of a small part of the TND along the [001] and [010] directions.

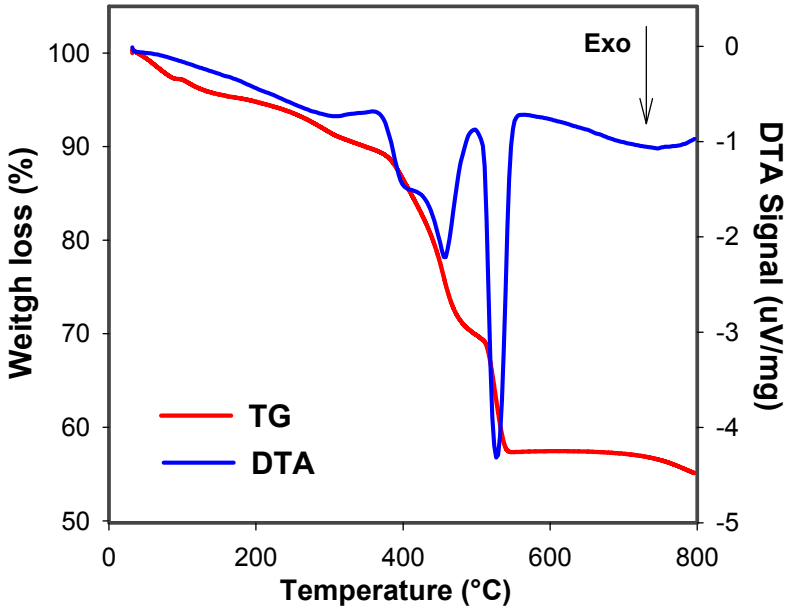

Figure S2. TGA and DTA curves of the as-synthesized TNDs (OM-TNDs).

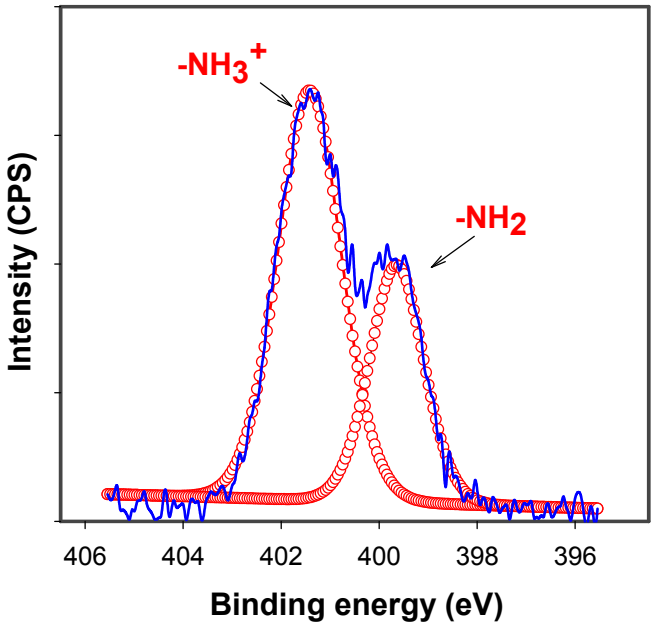

Figure S3. N1s XPS spectrum of as-synthesized TNDs (OM-TNDs).

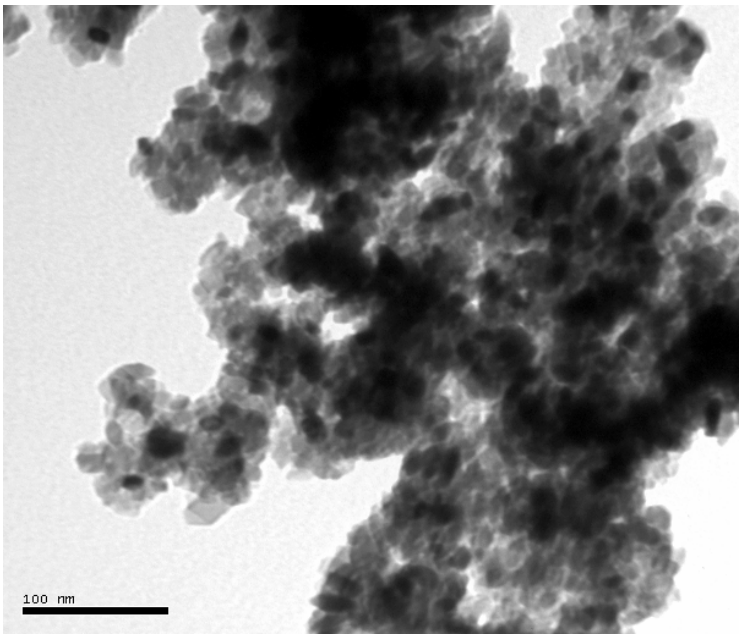

Figure S4. TEM image of the anatase TiO_2 particles obtained in the absence of OM.

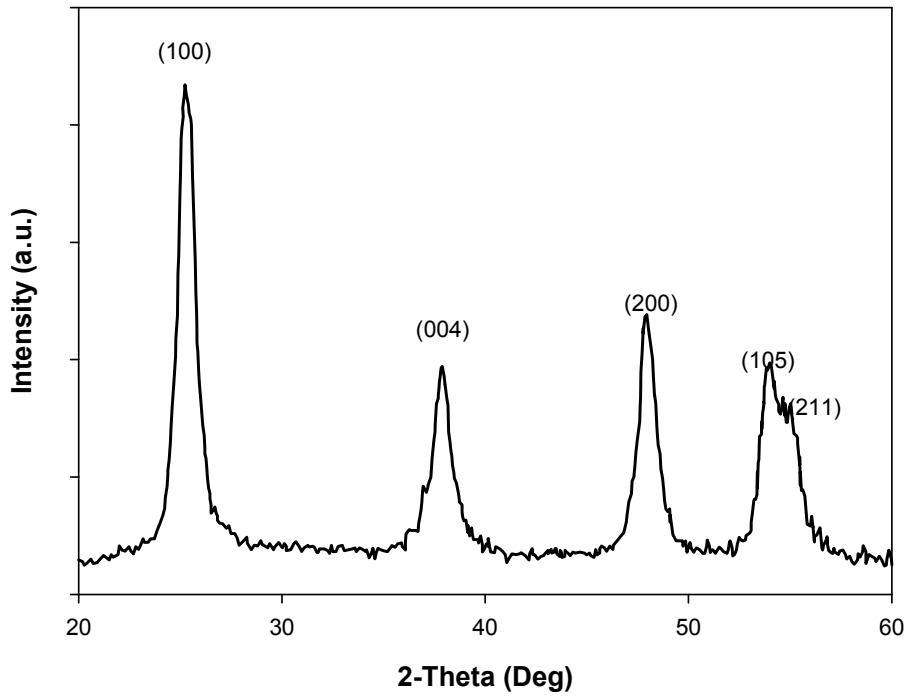

Figure S5. Powder XRD pattern of anatase TiO_2 particles obtained in the absence of OM.

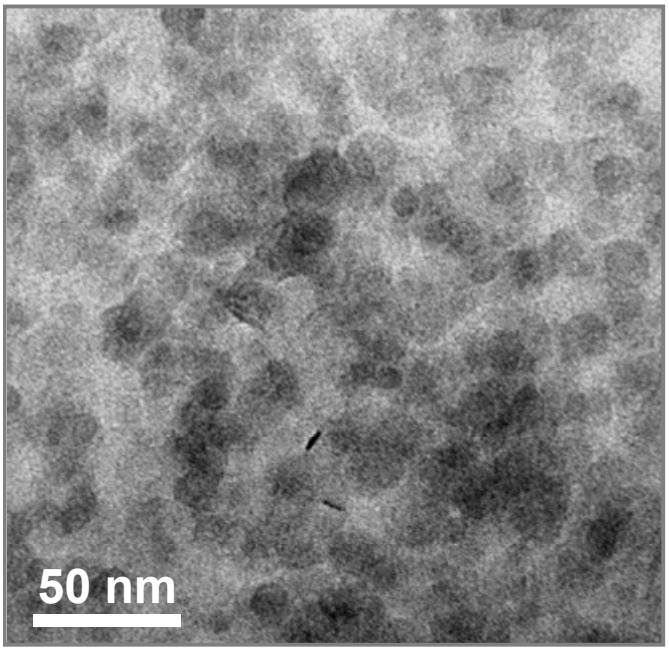

Figure S6. TEM image of 12 nm-diameter TNDs obtained by using 6 g of BA.

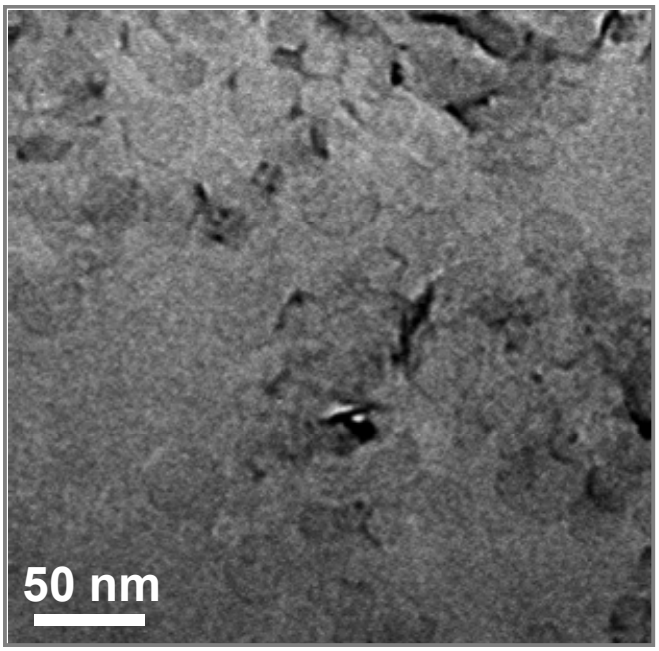

Figure S7. TEM image of 35 nm-diameter TNDs obtained by using 24 g of BA.

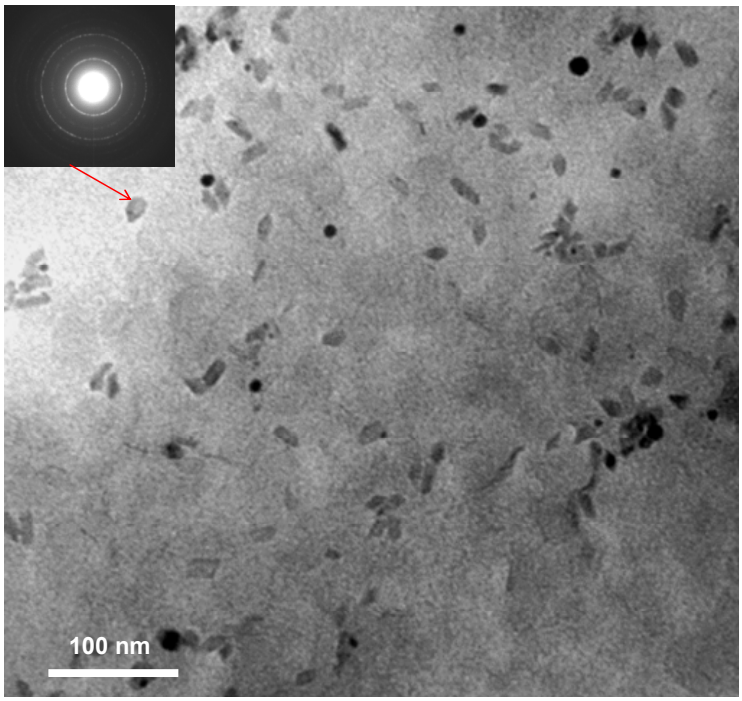

Figure S8. TEM image of a mixture of anatase TiO_2 and TNDs obtained by using 36 g of BA. Inset is the selected area electron diffraction of a single anatase TiO_2 particle (indicated by the arrow).

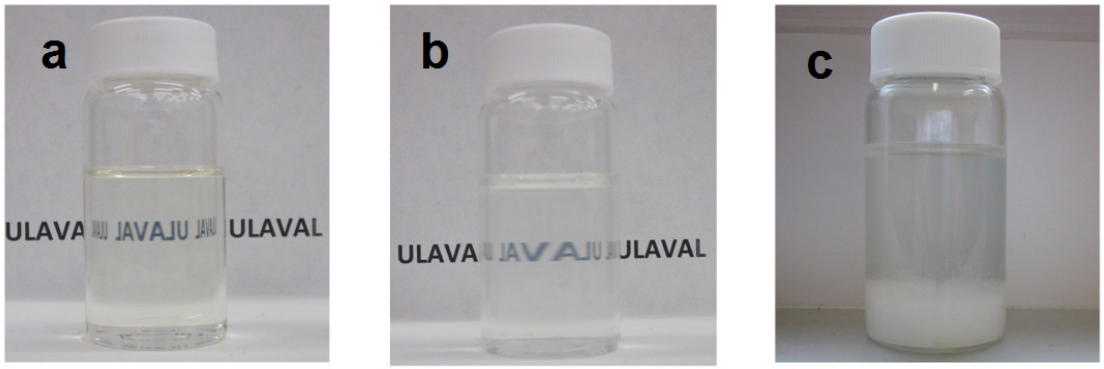

Figure S9. Photos of OM-TNDs dispersed in toluene (a), TEA-TNDs dispersed in water (b), and Ag^{+}-TNDs precipitated in water (c).

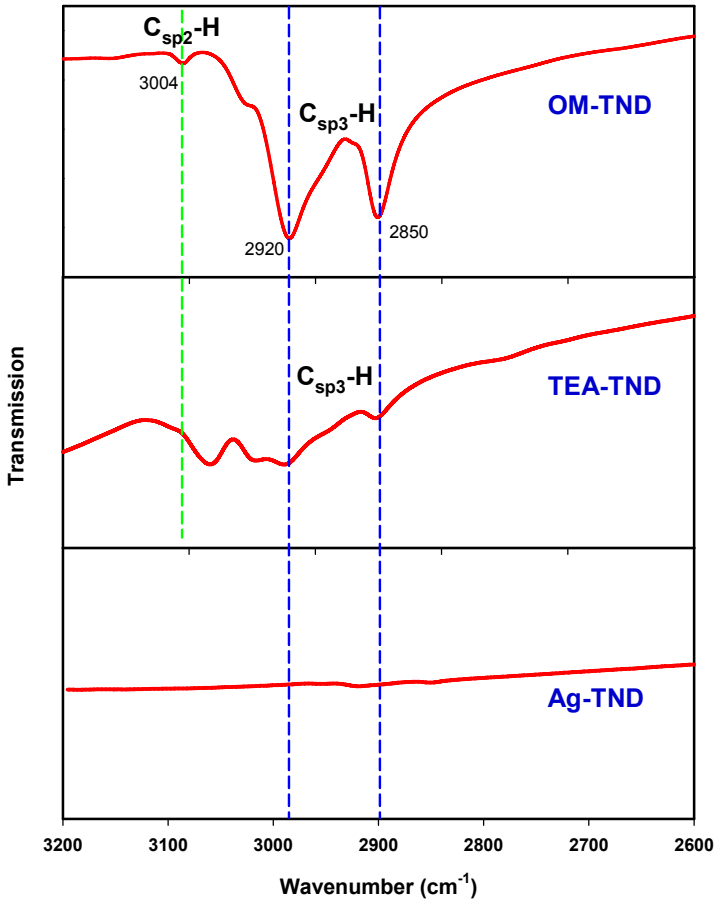

Figure S10. FTIR spectra of OM-TNDs (a), TEA-TNDs (b), and Ag^{+}-TNDs (c).

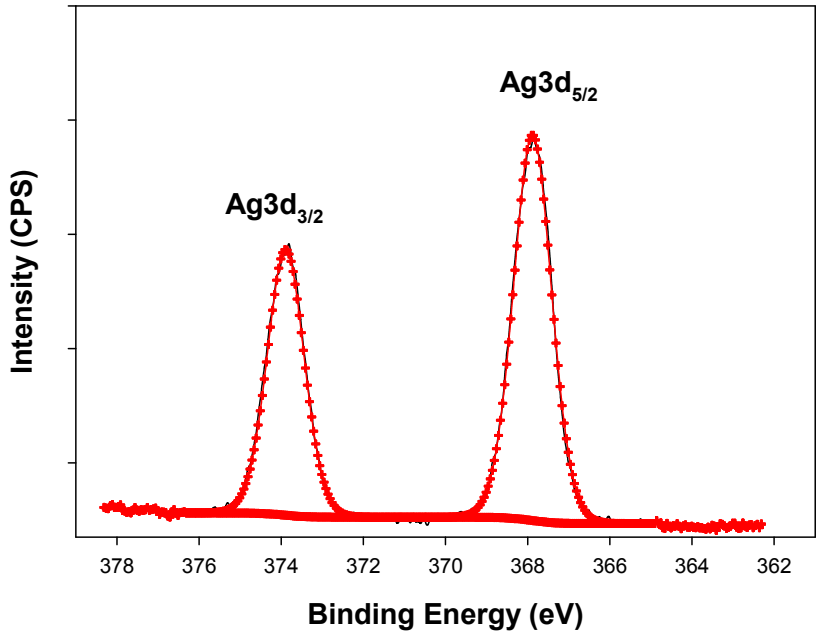

Figure S11A. $Ag3d_{5/2}$ XPS spectrum of mesoporous Ag_2O-TND-22 hybrids.

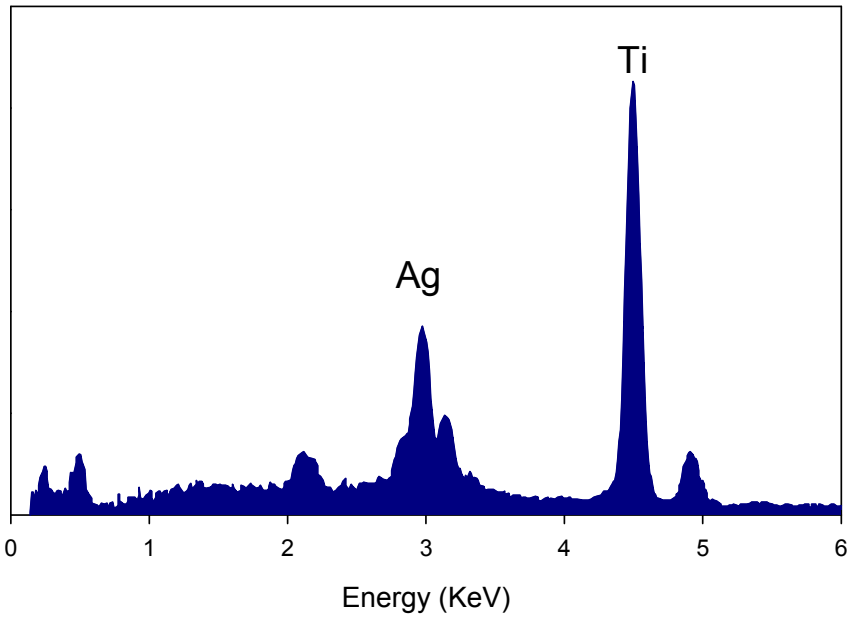

Figure S11B. EDS spectrum of mesoporous Ag_2O-TND-22 hybrids.

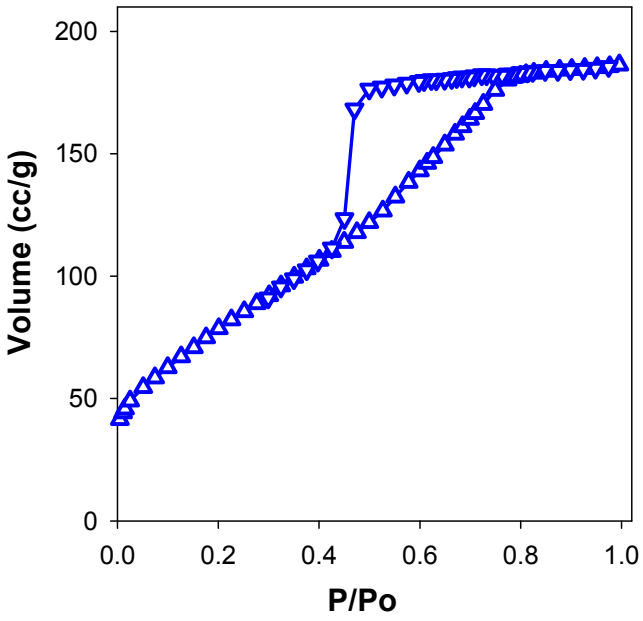

Figure S12. Nitrogen sorption isotherms measured at -196 °C of mesoporous Ag-TND-10 hybrids.

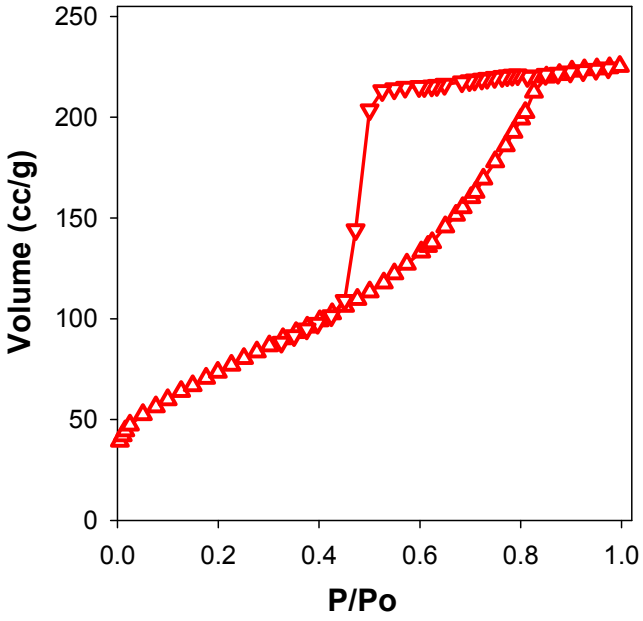

Figure S13. Nitrogen sorption isotherms measured at -196 °C of mesoporous Cu_xO-TND-22 hybrid.

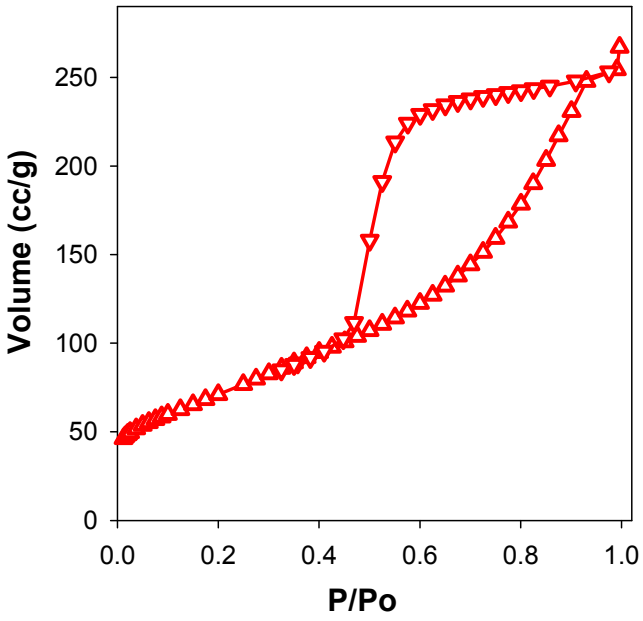

Figure S14. Nitrogen sorption isotherms measured at -196 °C of mesoporous CdS-TND-35 hybrid.

Table S1. Physicochemical parameters of the different mesoporous hybrids prepared using titanate nanodisks as building blocks (from N_2 sorption at -196 °C).

Samples	Surface area (S_{BET}, m^2/g)	Pore volume (V_{pore}, cc/g)	Pore diameter, nm
Ag_2O-TND-10	327	0.31	4.9
Ag_2O-TND-20	291	0.42	6.8
Ag_2O-TND-40	275	0.51	9.3
Ag-TND-10	290	0.28	3.7
Cu_xO-TND-20	277	0.35	5.2
CdS-TND-40	255	0.39	7.1

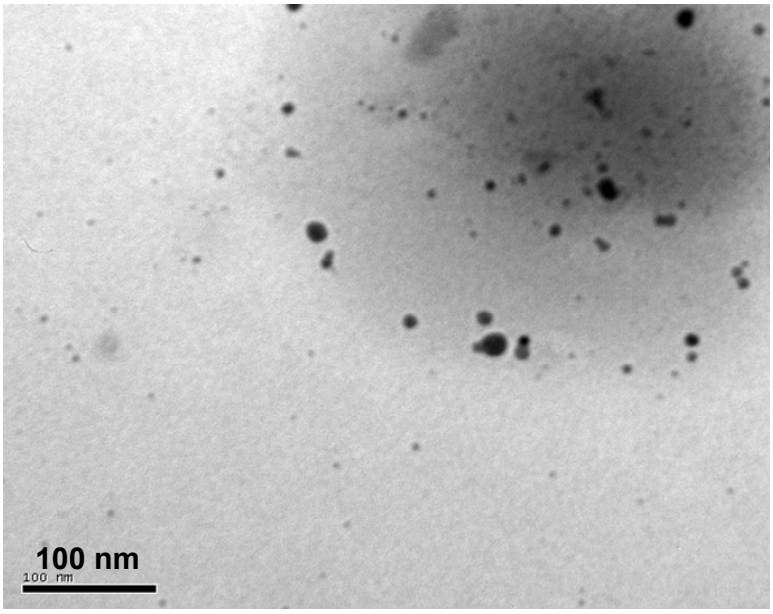

Figure S15. TEM image of PVP-stabilized Ag NPs.

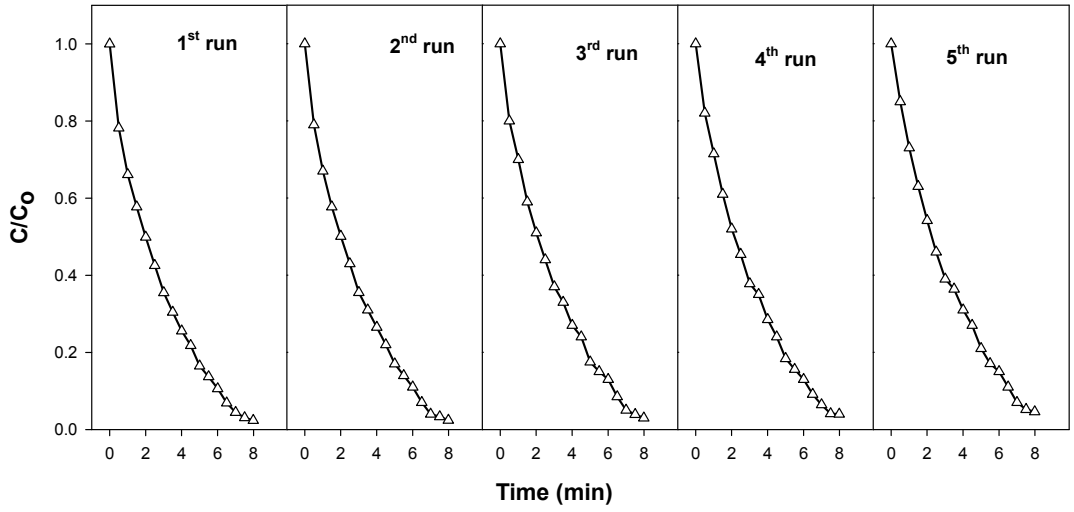

Figure S16. Variation of MB concentration against reaction time over the TND-stabilized Ag NPs catalyst in five consecutive reduction cycles.

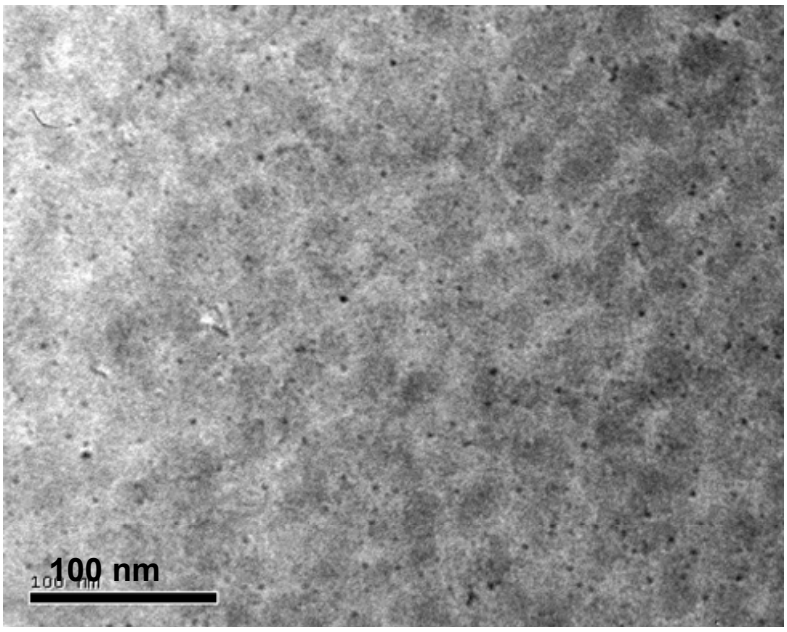

Figure S17A. TEM image of the Ag-TND hybrid colloids after five consecutive reduction cycles.

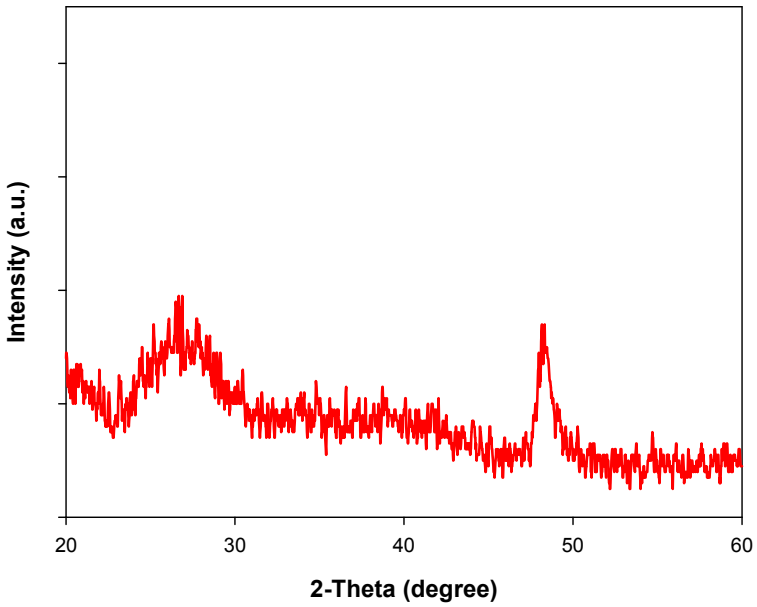

Figure S17B. Wide-angle XRD pattern of the Ag-TND hybrid colloids after five consecutive reduction cycles.

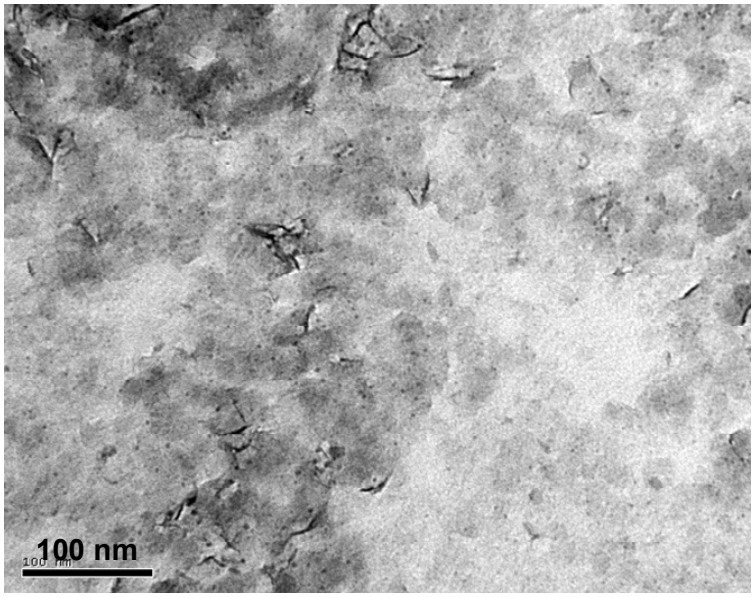

Figure S18. TEM image of Cu-TND hybrid.

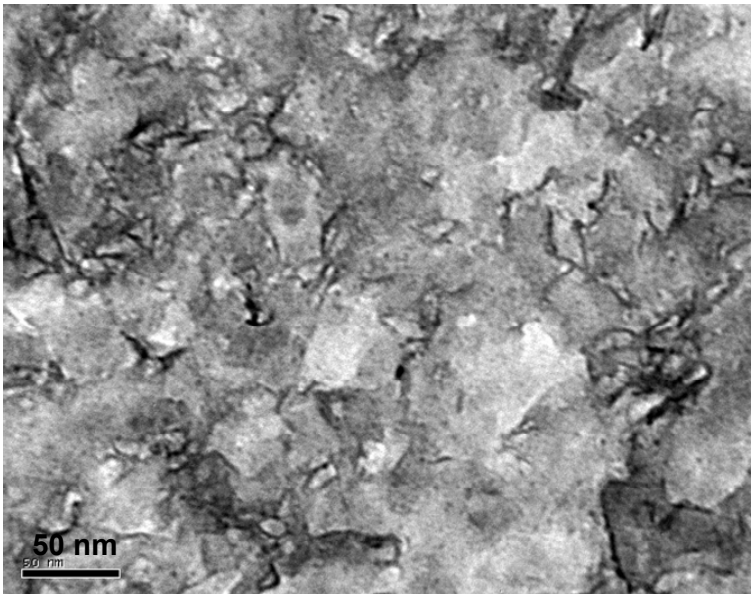

Figure S19. TEM image of Ni-TND hybrid.

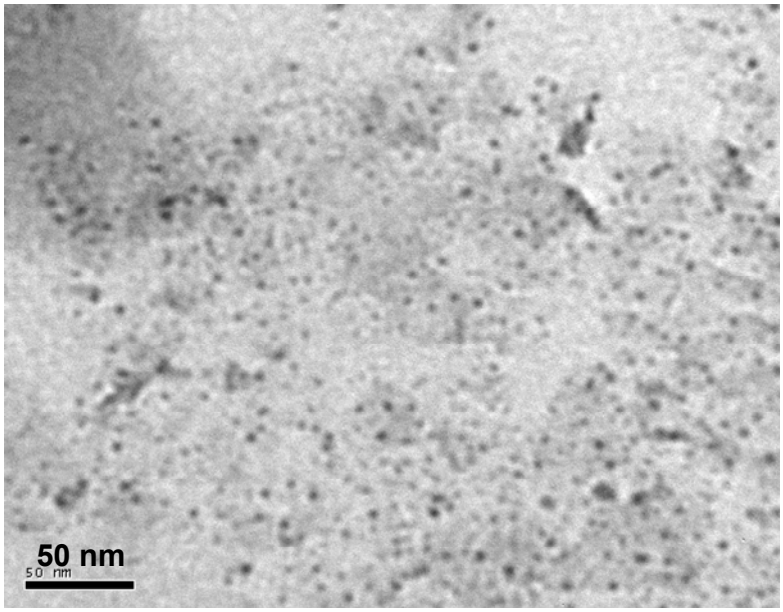

Figure S20. TEM image of AgBr-TND hybrids